DEFORMABLE GROUND CONTACT MODELING: AN OPTIMIZATION APPROACH

Jeff Reinbolt

EML 5595 – Mechanics of the Human Locomotor System – Final Project Report

INTRODUCTION

One of the most important choices made in creating a multi-body dynamic model of human movement involves how to handle the foot-ground interface. Ground contact models are essential to modeling changes in ground contact conditions (i.e., single vs. double support) and different movement tasks (i.e., gait vs. jumping). There are two main options for modeling ground contact: 1) constraint-based models and 2) deformable models.

Constraint-based methods confine the feet to the ground using revolute or weld joints. This approach requires separate models for different ground contact conditions. Constraint-based models permit the determination of constraining reaction forces and torques and facilitate analysis of induced acceleration and induced power.

Deformable ground contact methods use spring-damper elements, or units, as constraints. This approach allows the use of a single model regardless of changing ground contact conditions. Deformable models permit determination of discrete forces that prevent the foot from excessively penetrating the floor. However, these models complicate the induced acceleration and induced power analyses.

This final project report presents the development of a deformable ground contact modeling approach to reproduce experimental ground reactions given the experimental motion. Moreover, optimization techniques were implemented to determine a set of optimal ground contact model parameters.

METHODS

The approach was based upon an existing generic, parametric three-dimensional full-body kinematic model constructed with Autolev™ (Online Dynamics, Inc., Sunnyvale, CA) as a 14 segment, 27 degree-of-freedom linkage joined by a set of gimbal, universal, and pin joints (Appendix - Figure 1). The foot included a hindfoot segment linked to a toes segment with a weld joint. The foot-ground interface was modeled with four spring-damper units at the corners of the hindfoot and one unit at the distal end of the toes (Appendix - Figure 2), where these locations are similar to the Anderson and Pandy (1999) model.

The positions and velocities of each spring-damper attachment point were computed as functions of the model's generalized coordinates and patient-specific model parameters (i.e., segment lengths, joint positions, and joint orientations). Given the position of a particular attachment point, *i*, was known in the foot coordinate system, a series of transformation matrix multiplications (Appendix – Equation 1) was carried out to determine the attachment point position in the fixed coordinate system, *N*. Subsequently, the velocity of each attachment point was computed in *N* as well.

The position and velocity information was used to compute normal and tangential forces acting on each attachment point. Comparable to Hunt and Crossley's (1975) model for contact force between two colliding objects, each normal force was computed by a nonlinear equation (Appendix – Equation 2). In addition, the tangential forces were computed using Appendix – Equation 3, or Coulomb friction, applied opposite to the direction of sliding.

The individual attachment point forces were replaced by an equivalent set of forces and torques acting at the electrical center of the corresponding force plate for each foot model in *N*. The resulting three forces were simply the sum of each attachment point force component (Appendix – Equations 4-6). The three torques produced about the force plate's electrical center were also computed to complete the replacement (Appendix – Equations 7-9).

An optimization framework was formulated with Matlab (The MathWorks, Inc., Natick, MA) to reproduce ground reactions given the model's motion. The objective function was to minimize the error between recorded and simulated ground reactions. The design variables were the ground contact model parameters. As opposed to a nonlinear least squares algorithm to solve for spring stiffness, *k*, spring displacement raised to the power, *n*, damping coefficient, *c*, simultaneously in Appendix – Equation 2, a linear least squares approach was used to solve for *k* alone, where $n = 1$ and $c = 0$. This simplification allowed the optimization framework to be developed within the scope of the course project. Appendix – Equations 4-9 were combined into a large linear system of equations (including each time frame of data) to solve for *k* by inverting the coefficient matrix (right-hand side of Appendix – Equations 4-9 factored by *k*) and post-multiplying by the recorded ground reactions to be matched.

The ground contact optimization was used to solve five example applications. To demonstrate the computational model was well designed and written, synthetic attachment point positions and ground

reactions were implemented with uniform and subsequently random *k* values for each unit. As an intermediate step, random numerical noise was added to each synthetic data set. Finally, experimental data recorded from a normal subject's gait was applied.

Driving the model through a motion similar to gait generated four sets of synthetic ground reactions. By using a uniform *k* = 11,974 N/m, one set of noiseless synthetic data was created. By using random *k* values within $\pm$ 50% of the uniform *k*, a second set of noiseless data was produced. The third and fourth sets of synthetic data resulted from randomly varying the attachment point positions within $\pm$ 1 mm.

The ability of the ground contact optimization to recover the original model parameter (synthetic only – used to generate synthetic data) and the recorded ground reactions was assessed with normalized (i.e., unitless) root-mean-square (RMS) errors for each category. The *k* RMS errors were normalized by the uniform *k* = 11,974 N/m. The force RMS errors were normalized by the body weight (BW) = 689 N. The torque RMS errors were normalized by the product of body weight and height (BW*H) = 1,173 Nm.

RESULTS

The current ground contact optimization solutions decreased in accuracy with increased noise introduced into the data. For the noiseless synthetic data cases, each ground contact optimization precisely recovered the original model parameters and the recorded ground reactions to within an arbitrarily tight tolerance on the order of 2e-13% for *k* and 4e-14% for force and torque RMS errors (Appendix – Table 1 – first and second data sets). For synthetic data with noise cases, the RMS errors increased for both uniform *k* and random *k* cases (Appendix – Table 1 – third and fourth data sets). For the experimental data case, the RMS errors were categorically larger compared to the synthetic data cases (Appendix – Table 1 – fifth data set). Although it was not possible to assess the accuracy of the experimental *k* parameters, the *k* value of the posterior lateral unit was negative for each foot (Appendix – Table 2). The largest RMS errors occurred for the superior force (20% BW) and mediolateral torque (7% BW*H), which are much larger in recorded values compared to their orthogonal counterparts.

DISCUSSION

This final project report has presented the development of a deformable ground contact modeling approach to reproduce experimental ground reactions given the experimental motion. Through simplification of a nonlinear spring-damper model, a linear least squares approach was used to determine individual spring stiffness values for five units distributed under each foot. Uniting the foot-ground interface model with a full-body model will facilitate forward dynamic simulations of human movement.

Given the scope of the course project, there are several limitations inherent to the current model. Five out of ten experimental spring stiffness values were comparable to 40,000 N/m reported by Gilchrist and Winter (1996). However, the other values were roughly twice this magnitude or negative. The noiseless synthetic data results were promising. However, introduction of positional noise (on the order of $\pm$ 1 mm) significantly affected the recovery of spring stiffness values and ground reactions. In addition, the experimental RMS errors were considerably high. Kinematic noise certainly affects the computed ground reactions; as a result, the *k* values found for experimental data may not be reliable.

Future work is necessary to answer several relevant questions related to model fidelity and reliability. It is necessary to determine the accuracy of the foot sole location and shape based upon skin markers. The bottom of the model foot segment is flat and does not deform as a true foot. The optimal number and location of spring-damper units is not known. Obviously, five units place on the outside edge of the foot segment is not optimal. Excessive interpenetration of the foot edge with the ground lowers the associated spring stiffness, such as with both current posterior lateral units. Moreover, a smaller number of units raise the resulting spring stiffness values compared to many more units.

In conclusion, the current deformable ground contact model approach needs further development to determine trustworthy model parameters and ground reactions.

REFERENCES

1. Anderson, F.C. and Pandy, M.G. (1999) *Computer Methods in Biomechanics and Biomedical Engineering* **2**, 201-231.
2. Gilchrist, L.A. and Winter, D.A. (1996) *Journal of Biomechanics* **29**, 795-798.
3. Hunt, K.H. and Crossley, F.R.E. (1975) *ASME Journal of Applied Mechanics*, 440-445.

ACKNOWLEDGMENTS

This study was funded by Whitaker Foundation and NIH National Library of Medicine (R03 LM07332-01) grants to Professor B.J. Fregly and it was motivated by the EML 5595 course grade and Research Assistantship to the author. The author gratefully recognizes Professor Fregly for his project input and support.

APPENDIX

$$ {}^{i}_{N}T = {}^{Pelvis}_{N}T \; {}^{Femur}_{Pelvis}T \; {}^{Tibia}_{Femur}T \; {}^{Talus}_{Tibia}T \; {}^{Foot}_{Talus}T \; {}^{i}_{Foot}T $$

Equation 1. The transformation matrix multiplication to compute the position of spring-damper unit attachment point, *i*, in the fixed coordinate system, *N*.

$$ F_{normal} = k\, x^{n}\, (1 + c\, \dot{x}) $$

Equation 2. The nonlinear spring-damper normal force equation as a function of spring stiffness, *k*, spring displacement, *x*, raised to the power, *n*, damping coefficient, *c*, and first time derivative of spring displacement, $\dot{x}$.

$$ F_{tangent} = \mu\, F_{normal} $$

Equation 3. The Coulomb friction tangential force equation as a function of friction coefficient, μ, and normal force.

$$ (F_x)_{EC} = \sum_{i=1}^{5} (F_x)_i $$

Equation 4. The sum of the forces for individual attachment points, *i*, in the *x*-direction (anterior) replaced by the equivalent force acting on the electrical center, *EC*, of the corresponding force plate.

$$ (F_y)_{EC} = \sum_{i=1}^{5} (F_y)_i $$

Equation 5. The sum of the forces for individual attachment points, *i*, in the *y*-direction (superior) replaced by the equivalent force acting on the electrical center, *EC*, of the corresponding force plate.

$$ (F_z)_{EC} = \sum_{i=1}^{5} (F_z)_i $$

Equation 6. The sum of the forces for individual attachment points, *i*, in the *z*-direction (lateral) replaced by the equivalent force acting on the electrical center, *EC*, of the corresponding force plate.

$$ (T_x)_{EC} = \sum_{i=1}^{5} \left\{ -\left[(p_z)_i - (p_z)_{EC} \right] (F_y)_i + \left[(p_y)_i - (p_y)_{EC} \right] (F_z)_i \right\} $$

Equation 7. The sum of the torques about the *x*-direction (anteroposterior) at the electrical center, *EC*, of the corresponding force plate produced by forces (superior and lateral) acting on individual attachment points, *i*. The position of *EC* is given by $(p_x, p_y, p_z)_{EC}$ and the position of each *i* is given by $(p_x, p_y, p_z)_i$ in the fixed coordinate system.

$$ (T_y)_{EC} = \sum_{i=1}^{5} \left\{ \left[(p_z)_i - (p_z)_{EC} \right] (F_x)_i - \left[(p_x)_i - (p_x)_{EC} \right] (F_z)_i \right\} $$

Equation 8. The sum of the torques about the *y*-direction (longitudinal) at the electrical center, *EC*, of the corresponding force plate produced by forces (anterior and lateral) acting on individual attachment points, *i*. The position of *EC* is given by $(p_x, p_y, p_z)_{EC}$ and the position of each *i* is given by $(p_x, p_y, p_z)_i$ in the fixed coordinate system.

$$ (T_z)_{EC} = \sum_{i=1}^{5} \left\{ -\left[(p_y)_i - (p_y)_{EC} \right] (F_x)_i + \left[(p_x)_i - (p_x)_{EC} \right] (F_y)_i \right\} $$

Equation 9. The sum of the torques about the *z*-direction (mediolateral) at the electrical center, *EC*, of the corresponding force plate produced by forces (anterior and superior) acting on individual attachment points, *i*. The position of *EC* is given by $(p_x, p_y, p_z)_{EC}$ and the position of each *i* is given by $(p_x, p_y, p_z)_i$ in the fixed coordinate system.

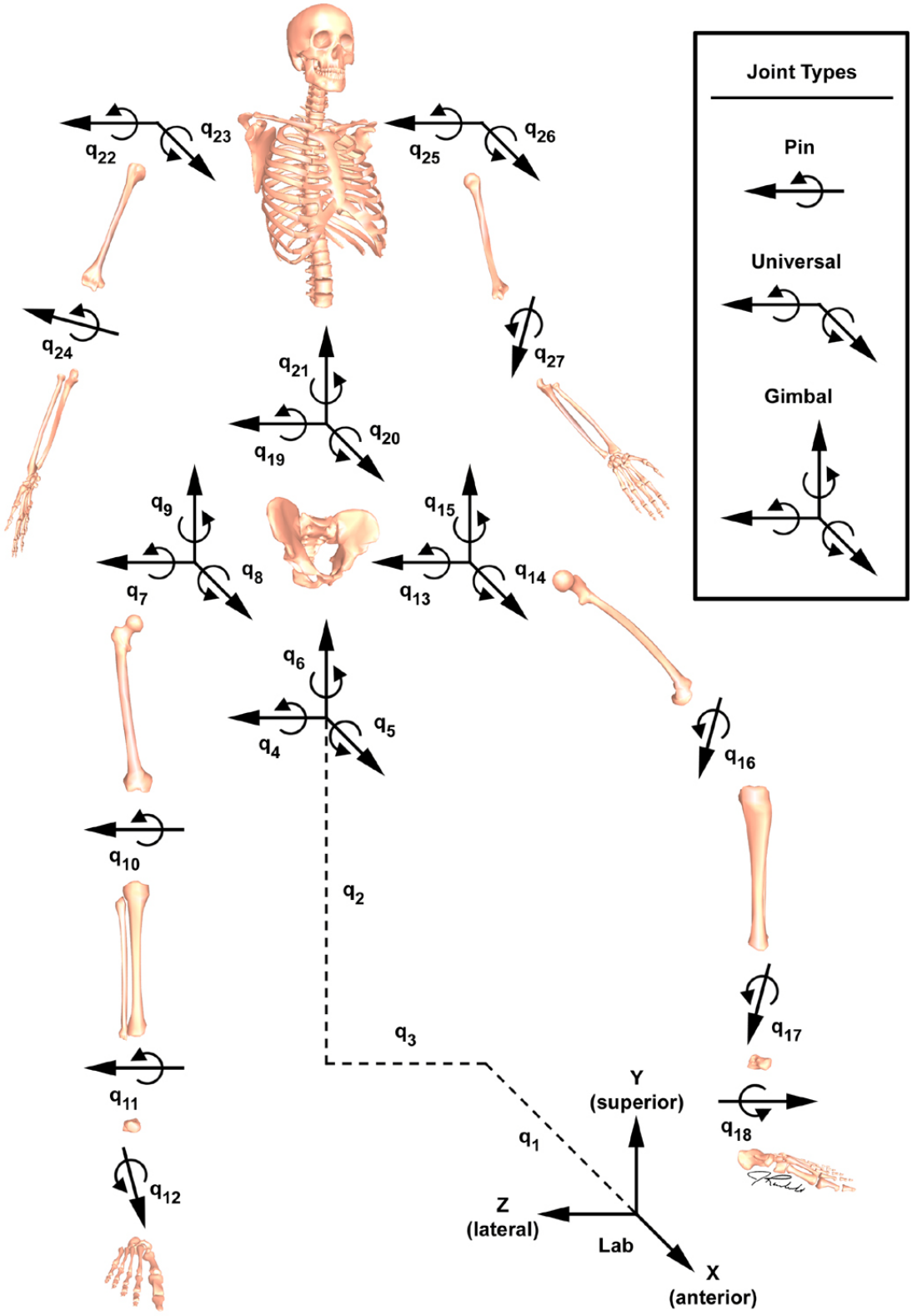

Figure 1. The three-dimensional, 14 segment, 27 degree-of-freedom full-body kinematic model linkage joined by a set of gimbal, universal, and pin joints.

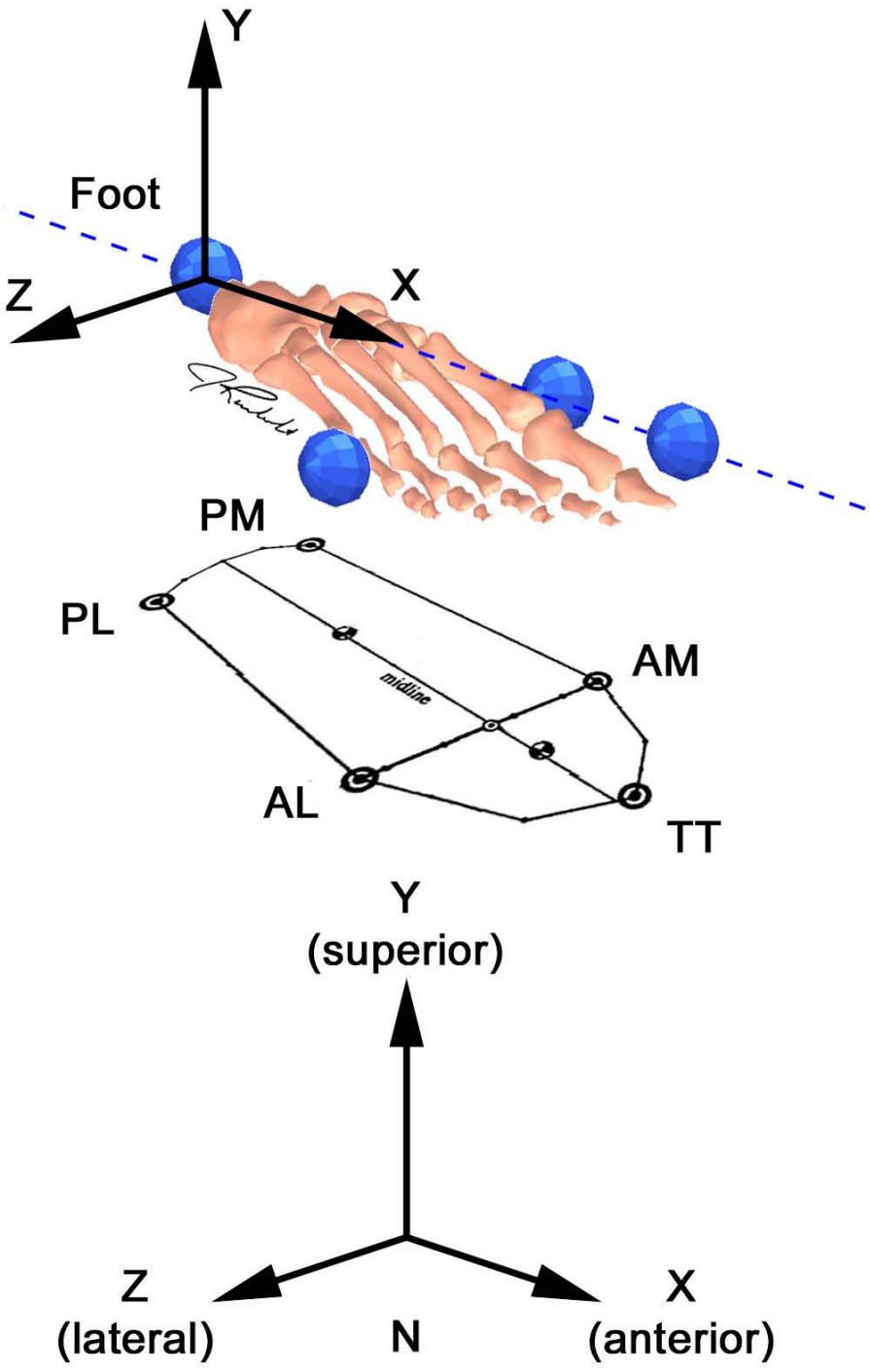

Figure 2. The foot coordinate system (top) defined by skin-based markers placed over the heel, toe, and beside the toe joint. The simulated sole of the foot (middle) with five spring-damper attachment points: posterior lateral (PL); posterior medial (PM); anterior lateral (AL); anterior medial (AM); and distal toe tip (TT). The skin-based markers, the foot coordinate system, and each attachment point are known in the laboratory fixed frame, N (bottom).

Table 1. Root-mean-square (RMS) errors between recorded and simulated ground contact model spring stiffness, *k*, and ground reactions for five example applications: 1) synthetic data without noise generated with uniform *k* values; 2) synthetic data without noise generated with random *k* values; 3) synthetic data with noise generated with uniform *k* values; 4) synthetic data with noise generated with random *k* values; and 5) experimental data collected from a normal subject's gait with unknown *k* values.

Data Type	RMS Error						
	k (% Uniform k)	Anterior Force (% BW)	Superior Force (% BW)	Lateral Force (% BW)	Anteroposterior Torque (% BW*H)	Longitudinal Torque (% BW*H)	Mediolateral Torque (% BW*H)
Synthetic without noise with uniform k	2.31e-13	2.55e-16	3.74e-14	2.21e-16	4.23e-15	1.01e-16	1.89e-14
Synthetic without noise with random k	2.32e-13	2.43e-16	3.33e-14	2.06e-16	3.73e-15	7.81e-17	1.48e-14
Synthetic with noise with uniform k	3.13	0.013	2.27	0.013	0.16	0.0045	0.74
Synthetic with noise with random k	6.59	0.015	2.52	0.014	0.21	0.0050	0.81
Experimental	n/a	6.46	20.26	1.83	3.35	0.29	7.09

Table 2. Experimental spring stiffness, *k*, values determined by the ground contact optimization.

Side	Unit Location	*k* (N/m)
Left	Posterior Lateral (PL)	-4277.15
	Posterior Medial (PM)	22106.33
	Anterior Lateral (AL)	23587.15
	Anterior Medial (AM)	70986.77
	Toe Tip (TT)	16315.52
Right	Posterior Lateral (PL)	-18437.78
	Posterior Medial (PM)	36800.79
	Anterior Lateral (AL)	82998.65
	Anterior Medial (AM)	-67927.68
	Toe Tip (TT)	13156.56